2020

Beam-Target Helicity Asymmetry E in K⁺Σ⁻ Photoproduction On The Neutron

N. Zachariou

K. P. Adhikari
Old Dominion University

M. Khachatryan
Old Dominion University, mkhachat@odu.edu

M. Mayer
Old Dominion University

Y. Prok
Old Dominion University, yprok@odu.edu

See next page for additional authors

Authors

N. Zachariou, K. P. Adhikari, M. Khachatryan, M. Mayer, Y. Prok, Et al., and CLAS Collaboration
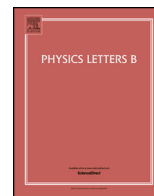
Beam–target helicity asymmetry E in $K^+\Sigma^-$ photoproduction on the neutron

The CLAS Collaboration

N. Zachariou [a],[*], D.P. Watts [a], J. Fleming [b], A.V. Sarantsev [c],[d], V.A. Nikonov [c],[d],
A. D'Angelo [w],[ai], M. Bashkanov [a], C. Hanretty [am],[as], T. Kageya [am], F.J. Klein [j], M. Lowry [am],
H. Lu [e], A. Sandorfi [am], X. Wei [am], I. Zonta [ai], K.P. Adhikari [ag],[1], S. Adhikari [r], M.J. Amaryan [ag],
G. Angelini [t], G. Asryan [au], H. Atac [al], L. Barion [u], C. Bass [am], M. Battaglieri [am],[v],
I. Bedlinskiy [ac], F. Benmokhtar [o], A. Bianconi [ap],[y], A.S. Biselli [p], F. Bossù [k], S. Boiarinov [am],
W.J. Briscoe [t], W.K. Brooks [an], D. Bulumulla [ag], V. Burkert [am], D.S. Carman [am], J.C. Carvajal [r],
A. Celentano [v], G. Charles [k],[2], P. Chatagnon [z], T. Chetry [ab], G. Ciullo [u],[q], P.L. Cole [aw],[3],
M. Contalbrigo [u], N. Dashyan [au], R. De Vita [v], A. Deur [am], S. Diehl [m], C. Djalali [af],[ak],
R. Dupre [z],[k],[f], H. Egiyan [am], M. Ehrhart [f], A. El Alaoui [an],[f], P. Eugenio [s], S. Fegan [aq],[4],
R. Fersch [l],[at], A. Filippi [x], G. Gavalian [am],[ag], N. Gevorgyan [au], Y. Ghandilyan [au], G.P. Gilfoyle [ah],
F.X. Girod [am],[m], W. Gohn [m], E. Golovatch [aj], R.W. Gothe [ak], K.A. Griffioen [at], M. Guidal [z],
K. Hafidi [f], H. Hakobyan [an],[au], M. Hattawy [ag], D. Heddle [l],[am], K. Hicks [af], D. Ho [i],
M. Holtrop [ad], Y. Ilieva [ak], D.G. Ireland [aq], B.S. Ishkhanov [aj], E.L. Isupov [aj], D. Jenkins [ar],
H.S. Jo [aa],[z], K. Joo [m], S.J. Joosten [f], D. Keller [as], M. Khachatryan [ag], A. Khanal [r],
M. Khandaker [ae],[5], C.W. Kim [t], W. Kim [aa], V. Kubarovsky [am], L. Lanza [w], M. Leali [ap],[y],
P. Lenisa [q],[u], K. Livingston [aq], I.J.D. MacGregor [aq], D. Marchand [z], N. Markov [m],
L. Marsicano [v], V. Mascagna [ao],[y],[6], M. Mayer [ag], B. McKinnon [aq], Z.E. Meziani [al],[f],
T. Mineeva [an], V. Mokeev [am],[aj], E. Munevar [am],[t], C. Munoz Camacho [z], P. Nadel Turonski [am],
T.R. O'Connell [m], M. Osipenko [v], A.I. Ostrovidov [s], M. Paolone [al],[ak], L.L. Pappalardo [q],[u],
K. Park [am], E. Pasyuk [am], P. Peng [as], W. Phelps [l], O. Pogorelko [ac], J. Poudel [ag], J.W. Price [g],
Y. Prok [ag],[l], A.J.R. Puckett [am],[7], B.A. Raue [r],[am], M. Ripani [v], A. Rizzo [w],[ai], G. Rosner [aq],
C. Salgado [ae], A. Schmidt [t], R.A. Schumacher [i], U. Shrestha [af], D. Sokhan [aq],[z], O. Soto [an],
N. Sparveris [al], I.I. Strakovsky [t], S. Strauch [ak], J.A. Tan [aa], N. Tyler [ak], M. Ungaro [am],
L. Venturelli [ap],[y], H. Voskanyan [au], E. Voutier [z], N.K. Walford [j], C.S. Whisnant [av],
M.H. Wood [h], J. Zhang [as], Z.W. Zhao [n],[as]

[a] *University of York, York YO10 5DD, United Kingdom*
[b] *University of Edinburgh, Edinburgh EH9 3FD, United Kingdom*
[c] *Helmholtz-Institut fuer Strahlen- und Kernphysik, Universität Bonn, 53115 Bonn, Germany*
[d] *National Research Centre "Kurchatov Institute", Petersburg Nuclear Physics Institute, Gatchina, 188300, Russia*
[e] *University of Iowa, Iowa City, IA 52242, United States of America*

[*] Corresponding author.
   E-mail address: nicholas@jlab.org (N. Zachariou).
[1] Current address: Mississippi State University, Mississippi State, MS 39762-5167, United States of America.
[2] Current address: Université Paris-Saclay, CNRS/IN2P3, IJCLab, 91405 Orsay, France.
[3] Current address: Lamar University, Beaumont, Texas 77710, United States of America.
[4] Current address: University of York, York YO10 5DD, United Kingdom.
[5] Current address: Idaho State University, Pocatello, Idaho 83209, United States of America.
[6] Current address: Università degli Studi di Brescia, 25123 Brescia, Italy.
[7] Current address: University of Connecticut, Storrs, Connecticut 06269, United States of America.

[f] *Argonne National Laboratory, Argonne, IL 60439, United States of America*
[g] *California State University, Dominguez Hills, Carson, CA 90747, United States of America*
[h] *Canisius College, Buffalo, NY, United States of America*
[i] *Carnegie Mellon University, Pittsburgh, PA 15213, United States of America*
[j] *Catholic University of America, Washington, D.C. 20064, United States of America*
[k] *IRFU, CEA, Université Paris-Saclay, F-91191 Gif-sur-Yvette, France*
[l] *Christopher Newport University, Newport News, VA 23606, United States of America*
[m] *University of Connecticut, Storrs, CT 06269, United States of America*
[n] *Duke University, Durham, NC 27708-0305, United States of America*
[o] *Duquesne University, 600 Forbes Avenue, Pittsburgh, PA 15282, United States of America*
[p] *Fairfield University, Fairfield CT 06824, United States of America*
[q] *Universita' di Ferrara, 44121 Ferrara, Italy*
[r] *Florida International University, Miami, FL 33199, United States of America*
[s] *Florida State University, Tallahassee, FL 32306, United States of America*
[t] *The George Washington University, Washington, DC 20052, United States of America*
[u] *INFN, Sezione di Ferrara, 44100 Ferrara, Italy*
[v] *INFN, Sezione di Genova, 16146 Genova, Italy*
[w] *INFN, Sezione di Roma Tor Vergata, 00133 Rome, Italy*
[x] *INFN, Sezione di Torino, 10125 Torino, Italy*
[y] *INFN, Sezione di Pavia, 27100 Pavia, Italy*
[z] *Université Paris-Saclay, CNRS/IN2P3, IJCLab, 91405 Orsay, France*
[aa] *Kyungpook National University, Daegu 41566, Republic of Korea*
[ab] *Mississippi State University, Mississippi State, MS 39762, United States of America*
[ac] *National Research Centre Kurchatov Institute - ITEP, Moscow, 117259, Russia*
[ad] *University of New Hampshire, Durham, NH 03824, United States of America*
[ae] *Norfolk State University, Norfolk, VA 23504, United States of America*
[af] *Ohio University, Athens, OH 45701, United States of America*
[ag] *Old Dominion University, Norfolk, VA 23529, United States of America*
[ah] *University of Richmond, Richmond, VA 23173, United States of America*
[ai] *Universita' di Roma Tor Vergata, 00133 Rome, Italy*
[aj] *Skobeltsyn Institute of Nuclear Physics, Lomonosov Moscow State University, 119234 Moscow, Russia*
[ak] *University of South Carolina, Columbia, SC 29208, United States of America*
[al] *Temple University, Philadelphia, PA 19122, United States of America*
[am] *Thomas Jefferson National Accelerator Facility, Newport News, VA 23606, United States of America*
[an] *Universidad Técnica Federico Santa María, Casilla 110-V Valparaíso, Chile*
[ao] *Università degli Studi dell'Insubria, 22100 Como, Italy*
[ap] *Università degli Studi di Brescia, 25123 Brescia, Italy*
[aq] *University of Glasgow, Glasgow G12 8QQ, United Kingdom*
[ar] *Virginia Tech, Blacksburg, VA 24061, United States of America*
[as] *University of Virginia, Charlottesville, VA 22901, United States of America*
[at] *College of William and Mary, Williamsburg, VA 23187, United States of America*
[au] *Yerevan Physics Institute, 375036 Yerevan, Armenia*
[av] *James Madison University, Harrisonburg, VA 22807, United States of America*
[aw] *Idaho State University, Pocatello, ID 83209, United States of America*

ARTICLE INFO

ABSTRACT

We report a measurement of a beam–target double-polarisation observable (E) for the $\vec{\gamma}\vec{n}(p) \to K^+\Sigma^-(p)$ reaction. The data were obtained impinging the circularly-polarised energy-tagged photon beam of Hall B at Jefferson Lab on a longitudinally-polarised frozen-spin hydrogen deuteride (HD) nuclear target. The E observable for an effective neutron target was determined for centre-of-mass energies $1.70 \leq W \leq 2.30$ GeV, with reaction products detected over a wide angular acceptance by the CLAS spectrometer. These new double-polarisation data give unique constraints on the strange decays of excited neutron states. Inclusion of the new data within the Bonn-Gatchina theoretical model results in significant changes for the extracted photocouplings of a number of established nucleon resonances. Possible improvements in the PWA description of the experimental data with additional "missing" resonance states, including the $N(2120)^{3/2^-}$ resonance, are also quantified.

Crown Copyright © 2020 Published by Elsevier B.V. This is an open access article under the CC BY license (http://creativecommons.org/licenses/by/4.0/). Funded by SCOAP^3.

1. Introduction

A central aim of hadron spectroscopy is to obtain a deeper understanding of how bound quark systems form from their fundamental partonic degrees of freedom (the quarks and gluons). The properties of such bound quark systems reveal valuable information on the underlying dynamics and their structure, while providing an important challenge to quantum chromodynamics (QCD) and its ability to fully describe the non-perturbative phenomena underlying hadron structure [1]. Although the nucleon is probably the most abundant bound quark system in the uni-

verse, our understanding of its dynamics and structure remains elusive. Specifically, the nucleonic excitation spectra evaluated in QCD-based approaches, (e.g. phenomenological constituent quark models [2–7], and lattice QCD [8–10]) predict many more excited states than currently established in experiment. Consequently, the "missing resonance" problem is an important focus for the world's electromagnetic beam facilities with the aim of achieving a better understanding of the nucleon from QCD.

The excited nucleon spectrum is characterised by interfering, broad, and overlapping resonances for all but the lowest mass states, making the determination of their properties (e.g. pho-

tocouplings, lifetimes, spins, parities, decay branches) challenging. The four complex amplitudes that determine the reaction dynamics at fixed kinematics [11] can be unambiguously determined from eight well-chosen combinations of observables, referred to as a "complete" measurement.[8] Therefore, kinematically (in W, and $\cos\theta$) complete and precise measurements of single- and double-polarisation observables using combinations of linearly- and circularly-polarised photon beams, transversely- and longitudinally-polarised targets, as well as the final state (recoiling) baryon polarimetry, in combination with partial wave analysis, are essential to resolve these states [11,13,17–19]. Furthermore, various resonances can have different photocouplings to neutron or proton targets [20,21] and also differ in their preferred decay branches, necessitating data from a wide range of final states such as $N\pi$, $K\Lambda$, $K\Sigma$, multiple meson decays such as $N\pi\pi$, and even vector meson decays such as $N\omega$ [3,11,22]. In fact, constituent quark model calculations [3] indicate that a number of currently "missing" or poorly established states could have escaped experimental constraint because of a stronger decay coupling to the strange sector ($K\Lambda$ or $K\Sigma$) rather than the (comparatively) well studied πN. Recent double-polarisation measurements from proton targets in the strange-decay sector have been particularly successful in establishing new states [23–32]. Disappointingly, the current database of such reactions for neutron targets is sparse, with only a single double-polarisation measurement obtained for $K^0\Lambda$ and $K^0\Sigma^0$ final states [33], obtained with quite limited statistics. In this work, we present the first measurement of the double-polarisation beam–target helicity asymmetry (E) for the reaction $\vec{\gamma}\vec{n} \to K^+\Sigma^-$, exploiting a circularly-polarised tagged-photon beam and a longitudinally-polarised hydrogen deuteride (HD) target, as an effective polarised-neutron target. This measurement is an important addition to the present world database for $K^+\Sigma^-$, which currently only comprises cross section determinations from CLAS [34,35] and a measurement of a single-polarisation observable, the beam-spin asymmetry (Σ), measured in a restricted kinematic range at LEPS [31], and it provides new constraints to the reaction mechanism.

The paper is organised as follows: Section 1 presents a short introduction, Section 2 describes the experimental setup, Section 3 introduces the polarisation observable E, and Section 4 gives an overview of the event selection and the analysis procedure to extract E. In Section 5, the new E data are compared with current theoretical models and the implications for the neutron excited states is discussed. Further details on the analysis procedure and systematic studies are presented in the online supplementary documentation accompanying this paper.

2. Experimental setup

The experiment was conducted at the Thomas Jefferson National Accelerator Facility (JLab) utilising the Continuous Electron Beam Accelerator Facility (CEBAF) and the CEBAF Large Acceptance Spectrometer (CLAS) [36] in Hall B (see Fig. 1). CLAS was a toroidal magnetic field analysing spectrometer covering polar angles between $\sim 8°$ and $140°$ with large azimuthal acceptance ($\sim 83\%$). The spectrometer was composed of a variety of tracking, time-of-flight, and calorimeter systems to provide particle identification and 4-vector determination for particles produced in electro- or photo-induced reactions.

The current data were obtained as part of the E06-101 experiment [37] (referred to as the g14 experiment), in which an energy-tagged polarised photon beam impinged on a 5-cm-long
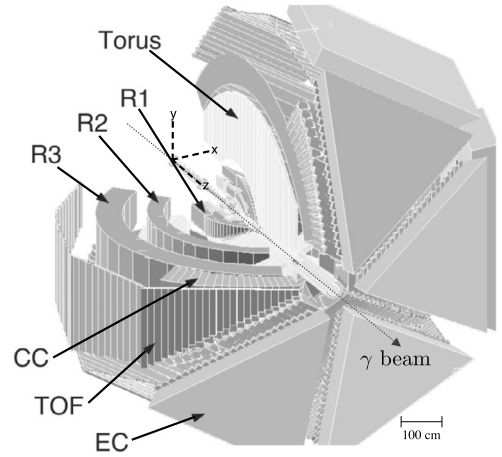

Fig. 1. A perspective view of CLAS showing the torus magnet, the three regions of drift chambers (R1–R3), the Cerenkov counters (CC), the time-of-flight detector (TOF), and the electromagnetic calorimeters (EC). The CLAS reference frame, also indicated here, was defined with the z axis along the beamline and the y axis perpendicular to the horizontal. Figure from Ref. [36].

solid target of polarised hydrogen deuteride (HD) [38,39] placed in the centre of CLAS. The energy-tagged (with energy resolution $\Delta E \sim 0.2\%$) and circularly-polarised photon beam was produced by impinging a longitudinally-polarised electron beam on a thin gold radiator, with post-bremsstrahlung electrons' momenta analysed in a magnetic tagging spectrometer [40]. The degree of photon polarisation varied between 20% and 85% depending on the incident photon energy, the electron-beam energy and the electron polarisation. The photon polarisation was determined using the Maximon and Olsen formula [41] taking into account the energy of the incident and bremsstrahlung electrons, as well as the polarisation of the incident electron beam, which was on average $P_e = 0.82 \pm 0.03$. This was periodically measured using the Hall B Møller polarimeter [42]. Information from the tagging spectrometer was used to identify and reconstruct the energy of the photon that initiated the reaction in CLAS.

During the experiment, the polarisation of the photon beam was flipped with ~ 960 Hz flip rate between the two helicity states. The vector polarisation for deuterons (i.e. bound neutrons) within the HD target was between 23% and 26% and it was continuously monitored using nuclear magnetic resonance measurements [38]. An in-beam cryostat that produced a 0.9 T holding field operating at 50 mK was used to hold the target polarisation, achieving relaxation times of about a year. The orientation of the target polarisation was also periodically flipped between directions parallel or anti-parallel to the incoming photon beam. The flipping of the photon and target polarisations allowed the determination of E using asymmetries, as described below, that significantly suppressed systematic uncertainties related to the detector acceptance. For more details on the experimental setup for the g14 experiment, see Ref. [33].

3. Polarisation observable E

Measurements employing a circularly-polarised photon beam in combination with a longitudinally-polarised target give access to the double-polarisation observable E. The differential cross section for the $\vec{\gamma}\vec{n} \to K^+\Sigma^-$ reaction for this case of a polarised beam and target is given by [17,43]:

$$\left(\frac{d\sigma}{d\Omega}\right) = \left(\frac{d\sigma}{d\Omega}\right)_0 (1 - P_T^{eff} P_\odot E), \tag{1}$$

where $\left(\frac{d\sigma}{d\Omega}\right)_0$ denotes the unpolarised differential cross section, P_T^{eff} denotes the effective target polarisation (accounting for events that originate from unpolarised material within the target cell), and $P_\odot$ the degree of circular photon polarisation.[9] The observable E is extracted from asymmetries, A, in the reaction yields arising from different orientations of the beam and target polarisations, for each kinematic bin $W = \sqrt{s}$ (s is the usual Mandelstam variable and denotes the total energy available in the reaction) and $\cos\theta_{K^+}^{cm}$, with $\theta_{K^+}^{cm}$ denoting the kaon polar angle in the center-of-mass frame:

$$A(W, \cos\theta_{K^+}^{cm}) = \frac{\left(\frac{d\sigma}{d\Omega}\right)^{\uparrow\downarrow} - \left(\frac{d\sigma}{d\Omega}\right)^{\uparrow\uparrow}}{\left(\frac{d\sigma}{d\Omega}\right)^{\uparrow\downarrow} + \left(\frac{d\sigma}{d\Omega}\right)^{\uparrow\uparrow}}, \qquad (2)$$

where $\uparrow\uparrow$ and $\uparrow\downarrow$ denote a parallel or anti-parallel orientation of the photon and target polarisations, respectively. The polarisation observable E is then given by

$$E = \frac{1}{P_T^{eff} P_\odot} A(W, \cos\theta_{K^+}^{cm}). \qquad (3)$$

This method allows the determination of E from the reaction yields for different combinations of the beam–target polarisations, while significantly reducing systematic effects from the detector acceptance.

4. Data analysis

Events containing a single K^+ and a single π^- in the final state (without further restrictions on any additional neutral tracks), were selected to provide a sample of $\gamma n(p) \to K^+\Sigma^-(p)$, where the Σ^- has decayed to $n\pi^-$ (with 99.8% branching ratio). Particle identification and photon selection were done following standard procedures adopted for E06-101 analyses, as discussed in Refs. [33] and [44].

The $K^+\pi^-$ yield was further analysed to select the reaction of interest and remove unwanted backgrounds. Due to limitations in the separation of pions and kaons at high momenta in CLAS, a fraction of events from the $\pi\pi$ final state were present in our yield. These were removed using kinematical cuts as described in the online supplementary documentation.

Further cuts were applied to the remaining event sample to eliminate background contributions. The kaon missing mass ($MM_{\gamma n \to K^+X}$) and the $K^+\pi^-$ missing mass ($MM_{\gamma n \to K^+\pi^-X}$) were calculated assuming a free neutron target (the systematic effect on the determination of E using this assumption was investigated as discussed later in this Section), and these are plotted in a two-dimensional histogram shown in Fig. 2. Events from the reaction of interest lie where the $MM_{\gamma n \to K^+X}$ corresponds to the nominal mass of the Σ^- and $MM_{\gamma n \to K^+\pi^-X}$ corresponds to the nominal mass of the neutron. The red lines in Fig. 2 indicate the two-dimensional cuts used to select the reaction of interest. The parameters of the two-dimensional cut were optimised to remove background contributions while maintaining a good event sample, as described below. Fig. 2 indicates the background channels, such as $\gamma p \to K^+\Lambda$, $\gamma p \to K^+\Sigma^0$, $\gamma p(n) \to K^*Y$ and $\gamma p(n) \to K^+\Sigma^*$, which can potentially contribute to the $\gamma n \to K^+\Sigma^-$ yield. To quantify the contribution of background events to the event sample, a comprehensive list of reactions that included the above
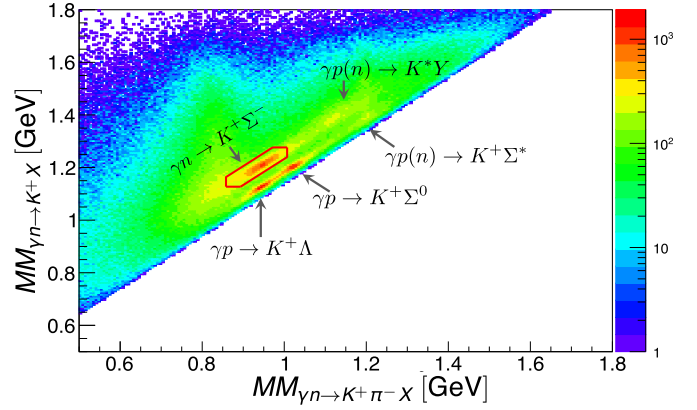

Fig. 2. Event distribution over $MM_{\gamma n \to K^+X}$ vs $MM_{\gamma n \to K^+\pi^-X}$. The regions where the different reaction channels contribute are indicated by the arrows on the figure. The region enclosed by the red boundary contains the selected events.

channels was simulated, processed through the CLAS acceptance and analysed identically to the $K^+\Sigma^-$ events. The final selection cuts applied to the data were optimised to reduce the background-to-total (B2T) ratio to the level of a few percent. With the tuned cuts (Fig. 2) the dominant background of $\gamma n \to K^+\Sigma^{*-}$ was reduced to B2T$_{\gamma n \to K^+\Sigma^{*-}} < 2\%$, while retaining a large fraction of the true yield. Contributions from $\gamma p(n) \to K^*Y$, were even smaller. The quantification of the background contributions allowed us to include their effects in the systematic uncertainty estimation, as described in the online supplementary documentation.

Measurements with an empty-target cell (i.e. without the HD target material) were used to quantify the contribution to the yield of events originating from the aluminium cooling wires or entrance/exit windows. These events originated from unpolarised nucleons (i.e. are associated with $P_T = 0$) and account must be made for the resulting "dilution" of the target polarisation. This was calculated based on the ratio of empty-target to full-target data within z-vertex cuts (with z along the beamline) that define the target cell (see Fig. 1 in Ref. [33], and online supplementary documentation). This dilution factor, D_F, was then used in the extraction of the helicity asymmetry from the data by determining the effective target polarisation: $P_T^{eff} = D_F P_T$. Our studies have shown no statistically significant variation in the kinematic dependence of the dilution factor and thus an overall constant value of $D_F = 0.728 \pm 0.003$ was used.

A thorough assessment of systematic effects in the extracted (E) observable was carried out, with more details provided in the online supplementary documentation. This included examining the effects of the particle identification cuts and reaction-vertex cuts (and therefore the effective target polarisation), as well as determining systematic uncertainties originating from the determination of the photon and target polarisations. Contributions from background channels as well as the Fermi motion of the target nucleon were extensively investigated by varying the reaction-reconstruction cuts, and these were the major contributor to the systematic uncertainty ($\Delta E_{background/Fermi}^{syst} = 0.087$). The systematic uncertainties arising from the Fermi motion of the target nucleon was investigated in detail using an independent (but low statistics) sample where the final-state neutron was identified. This absolute systematic uncertainty was estimated to be smaller than 0.02 and further details on these studies are provided in the supplementary documentation. Overall, no kinematic dependence of the systematic uncertainties was evident and therefore an upper estimate of a kinematic-independent uncertainty was established. The absolute systematic uncertainty associated with the determination of E was found to be $\Delta E^{syst} = 0.116$. In addition, a relative sys-

---

[9] The full cross-section equation indicates that two additional polarisation observables, P and H, are also accessible by studying the angular dependence of the decay products of the hyperon (taking into account the analysing power of Σ^-, $\alpha = 0.068$). In this analysis, the observables P and H are integrated out.

tematic (scale) uncertainty equal to $\Delta E^{syst}/E = 6.9\%$, which stems from the target (6%) and photon polarisation (3.4%), as well as the determination of the dilution factor (1%), was included in our systematics (see online supplementary materials for more details). Statistical uncertainties of E are driven by the values of target and photon polarisations, which scale the asymmetry uncertainty.

5. Results and discussion

The measured beam–target polarisation observable E is presented in Fig. 3 for six centre-of-mass energy (W) bins between 1.7 and 2.3 GeV and for six bins in K^+ center-of-mass angle ($\theta_{K^+}^{cm}$). The centre-of-mass frame is calculated assuming the target neutron at rest. However, the effect of Fermi motion on the value of W is small compared to the bin widths. The reported W value for each E_γ bin (see figure) is obtained from the event-weighted mean of the E_γ distribution. The angular bins are contiguous and have varying widths in response to the angular variation of the reaction yield. On average, the statistical sample per kinematic bin is of the order of 10^3, which results in an uncertainty of the asymmetry, $A(W, \cos\theta_{K^+}^{cm})$, of the order of 0.02. From this, the statistical uncertainty of E is of the order of 0.2, taking into account the effective target ($\sim 25\% \times 0.728$) and photon (30%-85%) polarisations. The experimental data show a positive value of E for most of the sampled bins. The measured values of E at the edges of our angular acceptance range ($\cos\theta_{K^+}^{c.m.} = -0.7$ and $\cos\theta_{K^+}^{c.m.} = 0.7$) are, on average, less than 0.5. As E must have a value of $+1$ at $\cos\theta_{K^+}^{cm} \to \pm 1$ to conserve angular momentum, the observable values outside of our acceptance range (i.e. between $\cos\theta_{K^+}^{c.m.} = 0.7$ and $\cos\theta_{K^+}^{c.m.} = 1$ for forward and between $\cos\theta_{K^+}^{c.m.} = -0.7$ and $\cos\theta_{K^+}^{c.m.} = -1$ for backward angles) must vary rapidly to reach 1. The curves in Fig. 3 are the predictions of the E observable from the Kaon-MAID-2000 [45] (dashed green), Kaon-Maid-2017 [46] (dotted magenta) and Bonn-Gatchina-2017 [47] (solid black) PWA models (see supplementary material for data included in the Bonn-Gatchina-2017 fit). It is clear that the models give rather divergent predictions for this observable, and none of the current solutions give consistent agreement with the experimental data over the sampled kinematic range. This suggests that the relevant photoproduction amplitudes are not well constrained by the current world-data, and that the new data have the potential to provide new information. The Bonn-Gatchina-2017 [47] solution is fitted to the entire database of meson photoproduction from the nucleon (see Ref. [48] for data sets used in PWA). In this solution the only direct $K^+\Sigma^-$ constraints in the database are from the cross-section determination [34,35].

In Fig. 4, the impact of including the new data of E in the Bonn-Gatchina database is explored. The predictions of E from the new fits (Bonn-Gatchina-2019) are shown by the dashed red lines and blue dotted lines.[10] It is seen that the new solution gives a much improved fit to the data (for comparison, the Bonn-Gatchina-2017 solution is repeated on this figure (solid black line)). The implications of the new Bonn-Gatchina-2019 fit for the properties of the excited states are shown in Table 1, where the helicity couplings calculated at the pole position are compared with previously published values [49]. In the new solution, the phase of the coupling residues – defined by the interference of the resonance with other contributions including non-resonance terms and tails from other states – between the $L_{IJ}^{K\Sigma} = S_{11}$ and P_{13} partial waves has changed substantially from earlier fits. In fact, this is now better constrained by data since the E observable allows separation of the helicity
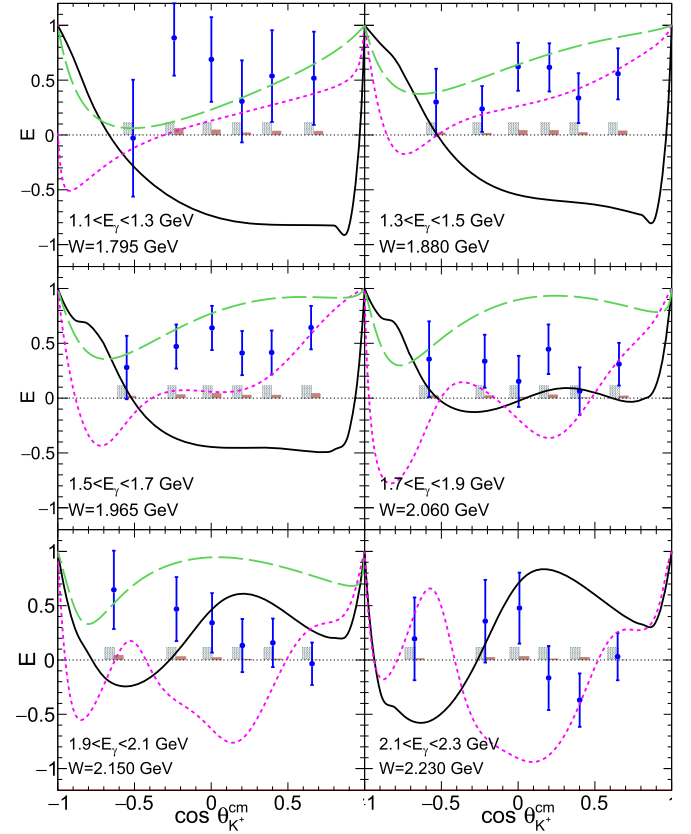

Fig. 3. Angular dependence of the beam–target double-polarisation observable E (with error bars indicating the combined statistical and absolute systematic uncertainties; the bar charts on zero axis show the magnitude of the absolute and scale systematic uncertainties at each point respectively) for the six center-of-mass energy W bins compared with the Kaon MAID 2000 (dashed green) and 2017 (dotted magenta), as well as predictions from Bonn-Gatchina (solid black). The event-weighted W value and the photon-energy bin are indicated in the panels.

projections 1/2 and 3/2 (corresponding to projections of the S_{11} and P_{13}, respectively). As a result, the new data produce significant changes in the extracted photocouplings of the individual states, particularly the $N(1720)^{3/2^+}$ and $N(1900)^{3/2^+}$ as indicated in Table 1.

The helicity 1/2 coupling of the $N(1720)^{3/2^+}$ state has the same magnitude as before but is rotated in phase by 90°, while the corresponding helicity coupling of the $N(1900)^{3/2^+}$ state has decreased by almost a factor 2. This results in a different behavior of the $N(1720)^{3/2^+}$ 1/2 helicity amplitude whose interference with the S_{11} partial wave defines the behavior of the E observable. The 3/2 helicity coupling of $N(1720)^{3/2^+}$ notably decreases and is rotated by 65° while the 3/2 helicity coupling of the $N(1900)^{3/2^+}$ state did not exhibit significant changes.

Furthermore, as shown in the left panels of Fig. 5, there is no significant difference in the description of the differential cross section between the new Bonn-Gatchina-2019 and the Bonn-Gatchina-2017 solutions, indicating that the cross section is not sensitive to the presence of D_{13}, nor the different photocouplings to individual states as discussed above. The new solutions suggest a small increase in the $K\Sigma$ cross section at backward kaon angles ($\cos\theta_{K^+}^{cm} < -0.7$), however, the sparse data at these angles do not allow us to draw any concrete conclusions. The improved agreement of the new solutions with the existing beam asymmetry data from LEPS [31] for $K\Sigma$ is also presented in Fig. 5. The existing LEPS data were not included in the Bonn-Gatchina-2017 solution, but are included in the solutions produced here, along with the current data on E.

---

[10] Note that the new fit also included the beam asymmetry data in very forward kaon kinematics from LEPS [31], which was not included in the previous Bonn-Gatchina-2017 fit. See Ref. [48] for a complete list of data used in this fit.
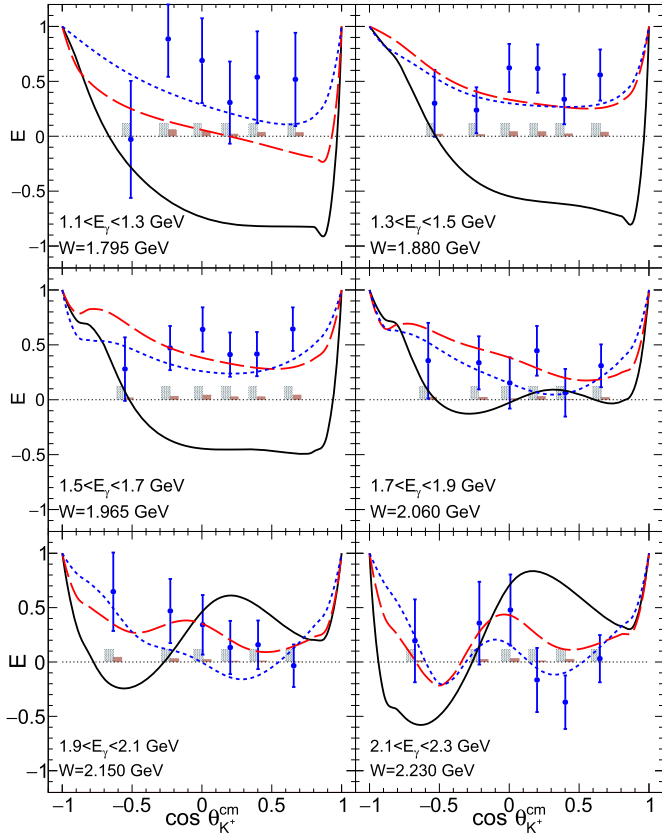
Fig. 4. The new Bonn-Gatchina description of the helicity asymmetry data. The error bars reflect the total statistical and absolute systematic uncertainty; the bar charts on zero axis show the magnitude of the absolute and scale systematic uncertainties at each point respectively. The Bonn-Gatchina-2017 solution [47] is shown with the solid black curves. The solution, with the new data on the helicity asymmetry included in the fit, is shown with dashed red lines. The solution with the added D_{13} state is shown with dotted blue lines.

Table 1

The γnN^* helicity couplings of nucleon states ($\text{GeV}^{-1/2}10^{-3}$) expressed in terms of the transverse helicity amplitudes and calculated as residues in the pole position. Previously reported values [49] are indicated in parentheses. Only resonances, which either are most important for the description of the new data or deviate by more than one standard deviation from the published results, are included.

	$A_{1/2}^n$	Phase	$A_{3/2}^n$	Phase
$N(1895)^{1/2^-}$	-20 ± 7	$50 \pm 20°$		
	(-15 ± 10)	$(60 \pm 25°)$		
$N(1720)^{3/2^+}$	-45 ± 15	$20 \pm 30°$	-35 ± 20	$-15 \pm 30°$
	(-25_{-15}^{+40})	$(-75 \pm 35°)$	(100 ± 35)	$(-80 \pm 35°)$
$N(1900)^{3/2^+}$	-45 ± 15	$-5 \pm 20°$	80 ± 12	$0 \pm 20°$
	(-98 ± 20)	$(-13 \pm 20°)$	(74 ± 15)	$(5 \pm 15°)$

The sensitivity of the new E data to missing or poorly established excited states was also explored within the Bonn-Gatchina framework. The database for reactions off neutron targets is much smaller than for the proton, so there is the potential to gain new sensitivities with the current data. There is significant current interest in gaining sensitivity to the $N(2120)^{3/2^-}$, a resonance predicted by many theoretical models of nucleon structure but still escaping proper experimental confirmation. The Bonn-Gatchina fits were repeated to include additional states, one at a time, with varying properties (e.g. helicity couplings). The best description of the new data was obtained when adding a D_{13} resonance of mass 2170 MeV. The results of this new fit (Bonn-Gatchina-2019-2) are shown by the dashed blue lines in Figs. 4 and 5. The new
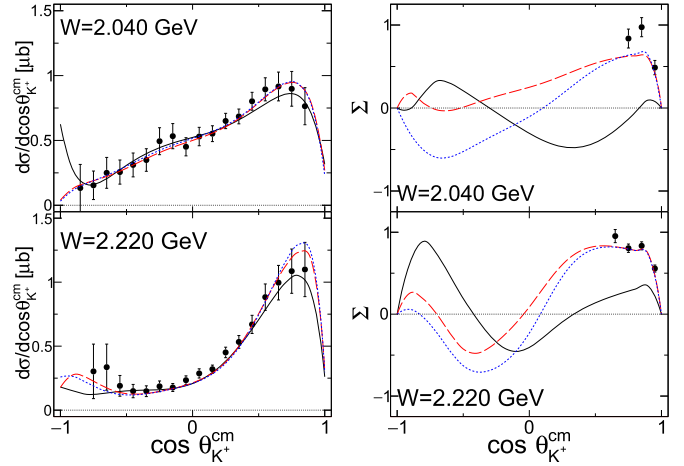

Fig. 5. The description of the differential cross section (data from [34]) (left) and the beam asymmetry (data from [31]) (right). The Bonn-Gatchina-2017 solution [47] is shown with the solid black curves. The solutions that includes the new data on the helicity asymmetry, E, as well as the beam-spin asymmetry data Σ from LEPS, are shown with the dashed red and dotted blue lines. The dotted blue line corresponds to the solution with an added D_{13} state.

E data are consistent with such a D_{13} contribution, which results in improved fits for many of the sampled W and K^+ center-of-momentum angle ranges. However, the level of improvement in the description of the E observable is not sufficient to make strong claims. Quantitatively, the total χ^2 was improved from 40.8 to 34.9, for 36 points, when the D_{13} state was included in the fit. The new solution does however provide a basis to explore sensitivities in other observables. The total χ^2 for the beam-spin asymmetry data from LEPS was significantly reduced from 124 to 84 for 36 points, when contributions from D_{13} resonance were included in the fit. The D_{13} is predicted to have a strong influence on the beam asymmetry and future measurements over a wider angular range could provide valuable constraints on its existence (e.g. see right panels in Fig. 5). Other possibilities were also explored. The inclusion of a missing $N(2060)^{5/2^-}$ marginally improved the agreement with data, particularly in the last energy bin, but was slightly worse in the bin which included the resonance central mass value. Furthermore, no improvement was obtained by including missing states with positive parity.

6. Summary

We present the first measurement of a double-polarisation beam–target observable (E) for the reaction $\vec{\gamma}\vec{n} \rightarrow K^+\Sigma^-$, employing a circularly-polarised photon beam and spin-polarised HD as an effective neutron target. The new E data are an important addition to the sparse world database constraining the strange decays of excited neutron states. Model predictions for the E observable in this channel were strongly divergent and none gave a good description of the new data over the full kinematic range. Fitting the new data in the framework of one of the models (Bonn-Gatchina) resulted in new constraints on the interference of the S_{11} and P_{13} partial waves, and significant changes in the extracted photocoupling of a number of resonance states, including the $N(1720)^{3/2^+}$, $N(1895)^{1/2^-}$, and $N(1900)^{3/2^+}$. Improved fits to the new E data could be obtained with the inclusion of a "missing" D_{13} resonance, although further measurements are clearly necessary to better establish this state. The determination of the beam spin asymmetry, Σ, for the reaction $\gamma n(p) \rightarrow K^+\Sigma^-(p)$ at backward angles could provide the necessary constraints for further investigations of this excited state.

Declaration of competing interest

Acknowledgements

Appendix A. Supplementary material

Supplementary material related to this article can be found online at https://doi.org/10.1016/j.physletb.2020.135662.

References

[1] I.G. Aznauryan, et al., Int. J. Mod. Phys. E 22 (2013) 1330015.
[2] S. Capstick, W. Roberts, Prog. Part. Nucl. Phys. 45 (2000) 241.
[3] S. Capstick, W. Roberts, Phys. Rev. D 58 (1998) 074011.
[4] S. Capstick, N. Isgur, Phys. Rev. D 34 (1986) 2809.
[5] U. Löring, B. Metsch, H. Petry, Eur. Phys. J. A 10 (2001) 395.
[6] L.Y. Glozman, W. Plessas, K. Varga, R.F. Wagenbrunn, Phys. Rev. D 58 (1998) 094030.
[7] M.M. Giannini, E. Santopinto, A. Vassallo, Eur. Phys. J. A 12 (2001) 447.
[8] R.G. Edwards, J.J. Dudek, D.G. Richards, S.J. Wallace, Phys. Rev. D 84 (2011) 074508.
[9] J. Dudek, R. Edwards, Phys. Rev. D 85 (2012) 054016.
[10] R.G. Edwards, N. Mathur, D.G. Richards, S.J. Wallace, Phys. Rev. D 87 (2013) 054506.
[11] W.-T. Chiang, F. Tabakin, Phys. Rev. C 55 (1997) 2054.
[12] T. Vrancx, J. Ryckebusch, T. Van Cuyck, P. Vancraeyveld, Phys. Rev. C 87 (2013) 055205.
[13] J. Nys, J. Ryckebusch, D.G. Ireland, D.I. Glazier, Phys. Lett. B 759 (2016) 260.
[14] D.G. Ireland, Phys. Rev. C 82 (2010) 025204.
[15] Y. Wunderlich, R. Beck, L. Tiator, Phys. Rev. C 89 (2014) 055203.
[16] L. Tiator, Bled Workshops Phys. 13 (2012) 55, arXiv:1211.3927 [nucl-th].
[17] A.M. Sandorfi, S. Hoblit, H. Kamano, T.S.H. Lee, J. Phys. G 38 (2011) 053001.
[18] C.G. Fasano, F. Tabakin, B. Saghai, Phys. Rev. C 46 (1992) 2430.
[19] G. Keaton, R. Workman, Phys. Rev. C 54 (1996) 1437.
[20] A.M. Sandorfi, S. Hoblit, Nucl. Phys. A 914 (2013) 538.
[21] T. Mart, C. Bennhold, C.E. Hyde-Wright, Phys. Rev. C 51 (1995) 1074(R).
[22] S. Capstick, W. Roberts, Phys. Rev. D 57 (1998) 4301.
[23] K.H. Glander, et al., Eur. Phys. J. A 19 (2004) 251.
[24] R. Castelijns, et al., Eur. Phys. J. A 35 (2008) 39.
[25] M. Nanova, et al., Eur. Phys. J. A 35 (2008) 333.
[26] R. Bradford, et al., Phys. Rev. C 73 (2006) 035202.
[27] M.E. McCracken, et al., Phys. Rev. C 81 (2010) 025201.
[28] M. Sumihama, et al., Phys. Rev. C 73 (2006) 035214.
[29] J.W.C. McNabb, et al., Phys. Rev. C 69 (2004) 042201.
[30] A. Lleres, et al., Eur. Phys. J. A 31 (2007) 79.
[31] H. Kohri, et al., Phys. Rev. Lett. 97 (2006) 082003.
[32] C.A. Paterson, Phys. Rev. C 93 (2016) 065201.
[33] D. Ho, et al., Phys. Rev. C 98 (2018) 045205.
[34] S.A. Pereira, et al., Phys. Lett. B 688 (2010) 289.
[35] N. Compton, et al., Phys. Rev. C 96 (2017) 065201.
[36] B.A. Mecking, et al., Nucl. Instrum. Methods A 503 (2003) 513.
[37] K. Ardashev, et al., JLab Proposal PR06-101, www.jlab.prg/exp_prog/proposals/06/PR06-101.pdf.
[38] M. Lowry, et al., Nucl. Instrum. Methods A 815 (2016) 31.
[39] C.D. Bass, et al., Nucl. Instrum. Methods 737 (2014) 107.
[40] D.I. Sober, et al., Nucl. Instrum. Methods 440 (2000) 263.
[41] H. Olsen, L. Maximon, Phys. Rev. 114 (1959) 887.
[42] J.M. Grames, et al., Phys. Rev. Spec. Top., Accel. Beams 7 (2004) 042802.
[43] I.S. Barker, A. Donnachie, J.K. Storrow, Nucl. Phys. B 95 (1975) 347.
[44] D. Ho, et al., Phys. Rev. Lett. 118 (2017) 242002.
[45] T. Mart, C. Bennhold, Phys. Rev. C 61 (1999) 012201.
[46] T. Mart, AIP Conf. Proc. 1862 (2017) 020001.
[47] A.V. Anisovich, et al., Phys. Lett. B 772 (2017) 247.
[48] A.V. Sarantsev, https://pwa.hiskp.uni-bonn.de/.
[49] A.V. Anisovich, et al., Phys. Rev. C 96 (2017) 055202.